nature neuroscience

ARTICLES

https://doi.org/10.1038/s41593-019-0511-3

Neuronal network activity controls microglial process surveillance in awake mice via norepinephrine signaling

Yong U. Liu[1], Yanlu Ying[1], Yujiao Li[1], Ukpong B. Eyo[1,2], Tingjun Chen[1], Jiaying Zheng[1], Anthony D. Umpierre[1], Jia Zhu[1], Dale B. Bosco[1], Hailong Dong[3] and Long-Jun Wu[1,4,5*]

Microglia dynamically survey the brain parenchyma. Microglial processes interact with neuronal elements; however, what role neuronal network activity plays in regulating microglial dynamics is not entirely clear. Most studies of microglial dynamics use either slice preparations or in vivo imaging in anesthetized mice. Here we demonstrate that microglia in awake mice have a relatively reduced process area and surveillance territory and that reduced neuronal activity under general anesthesia increases microglial process velocity, extension and territory surveillance. Similarly, reductions in local neuronal activity through sensory deprivation or optogenetic inhibition increase microglial process surveillance. Using pharmacological and chemogenetic approaches, we demonstrate that reduced norepinephrine signaling is necessary for these increases in microglial process surveillance. These findings indicate that under basal physiological conditions, noradrenergic tone in awake mice suppresses microglial process surveillance. Our results emphasize the importance of awake imaging for studying microglia–neuron interactions and demonstrate how neuronal activity influences microglial process dynamics.

Microglia are the resident immune cells of the CNS that interact with neuronal elements in the brain parenchyma[1–3]. Under normal conditions, microglia participate in synaptic pruning during brain development and in synaptic remodeling during learning[4,5]. Within neurological disorders such as pain, stroke, epilepsy, autoimmune diseases and neurodegeneration, microglia play key roles in pathology and can exert either detrimental or beneficial effects[6]. Multiple lines of evidence suggest that contact between microglial processes and neuronal dendrites can lead to changes in neuronal structure and function. Particularly during early developmental periods, microglial process contact can induce filipodia outgrowth from dendrites[7,8]. Conversely, in later development, microglial contact results in a higher probability of spine elimination[9]. This later interaction may be a key component of synaptic pruning and neuronal circuit formation[8,10]. In the mature brain, microglia can promote spine formation via BDNF signaling and thereby interact with the molecular mechanisms of learning and memory[11]. In addition, microglial processes can enhance dendritic calcium activity and may influence neuronal synchrony at the population level[12]. While microglial contact can influence neuronal structure and function across the developmental lifespan, it is unclear how microglial process dynamics are regulated in the basal state, particularly in the awake animal.

As surveilling immune cells, microglia dynamically respond to changes in the microenvironment with their remarkably motile processes[13–15]. To date, most studies of microglial process dynamics have occurred in slice preparations or under the constraints of general anesthesia in vivo. These studies showed that following laser-induced injury, local microglia quickly respond to damage by extending processes to isolate the injury site via a signaling mechanism comprising ATP and the $P2Y_{12}$ receptor (encoded by *Pty12* (also known as *P2ry12*))[13,14,16,17]. In addition, suppression of the neuronal network via tetrodotoxin (TTX) results in either reduced microglial–neuron contact[18] or no significant changes in microglial process surveillance[13]. Conversely, enhancements of the neuronal network via interneuron inhibition can lead to increases in process sampling[13]. Under more extreme circumstances, suprathreshold neuronal activity or acute seizure induction can further induce microglial process extension and convergence toward hyperactive neurons[19,20]. Thus, dynamic microglial processes are able to sense brain injury and neuronal activity in basal and disease contexts. More specifically, microglial process dynamics appear to follow activity-dependent patterns in anesthetized animals.

Despite the importance of microglial process dynamics in neuronal interactions, we currently do not know how microglial processes behave under the most physiologically relevant conditions (that is, in the awake state). Using in vivo two-photon imaging in awake mice, we surprisingly find that microglial processes are less dynamic and survey a smaller territory before neuronal activity is suppressed by general anesthesia. In awake animals, other methods of neuronal suppression, including sensory deprivation (whisker trimming) and optogenetic inhibition, mimicked the relative increase in microglial process surveillance. We found that adrenergic, but not purinergic, signaling controls the microglial surveillance phenotype observed in the awake state. Accordingly, in the awake state, pharmacological inhibition of β_2-adrenergic receptors or chemogenetic reductions of norepinephrine (NE) release from the locus coeruleus (LC) resulted in microglial process extension and increased surveillance territory. Thus, under awake conditions, microglial processes have constrained dynamics set by tonic NE tone. Under anesthesia, loss of NE tone becomes permissive for increasing microglia surveillance. Our findings in the awake animal demonstrate that microglial

[1]Department of Neurology, Mayo Clinic, Rochester, MN, USA. [2]Department of Neuroscience and Center for Brain Immunology and Glia, University of Virginia, Charlottesville, VA, USA. [3]Department of Anesthesiology, Xijing Hospital, Fourth Military Medical University, Xi'an, China. [4]Department of Neuroscience, Mayo Clinic, Jacksonville, FL, USA. [5]Department of Immunology, Mayo Clinic, Rochester, MN, USA. *e-mail: wu.longjun@mayo.edu

dynamics cannot be dictated by neuronal activity through a linear relationship. Instead, we advance a theory that microglial dynamics follow a 'U-shape' model of dynamics in response to neuronal activity via noradrenergic signaling.

Results

Microglial process surveillance increases after general anesthesia. Microglial processes extend and retract to survey the brain parenchyma. We first investigated how microglial process dynamics behave in the awake state using heterozygous mice expressing green fluorescent protein (GFP) under the control of the fractalkine receptor (*Cx3cr1*$^{GFP/+}$ mice) to visualize microglia in the somatosensory cortex (Supplementary Fig. 1a–d). After recovery from cranial window surgery (2–4 weeks), mice were trained to freely move on a custom-made, rotating treadmill while head restrained (Supplementary Fig. 1a). Using in vivo two-photon imaging, we observed that microglial processes maintain a relatively stable territory of surveillance in awake animals (Supplementary Fig. 1e–g).

We initially hypothesized that microglial process surveillance is dependent on neuronal activity, and would therefore be attenuated by general anesthesia. However, when isoflurane (1.2% in oxygen, 700 ml min^{-1}) was applied to the animal via a nose cone, we surprisingly observed that microglial processes began to extend and occupy a greater area of brain parenchyma, herein termed process surveillance (Fig. 1a,b; Supplementary Video 1). Increased process surveillance was initiated a few minutes after isoflurane induction and reached peak levels after 20–30 min. As expected, neuronal network activity in the cortex was strongly suppressed immediately after isoflurane induction, as determined by dampened calcium spikes in GCaMP6s-expressing cortical neurons (Fig. 1a,b; Supplementary Fig. 2a–d; Supplementary Video 2) and by in vivo electrophysiology showing slow wave activity (Supplementary Fig. 2e,f). We found that 10 min of isoflurane administration was sufficient to initiate an increase in microglial process surveillance that persisted for at least 50 min after isoflurane cessation (Supplementary Fig. 3). Thus, increases in microglial process surveillance represent a delayed but persistent response to the suppression of cortical network activity. Accompanying their increased process surveillance, microglia also exhibited faster process movement velocity (Fig. 1c) and more intricate ramified morphology, as demonstrated by a Sholl analysis and measurements of process lengths and number of branch points (Fig. 1e–g). These results reveal that isoflurane anesthesia enhances rather than inhibits microglial process dynamics.

Among other targets, isoflurane can inhibit the microglial two-pore domain potassium channel THIK-1, which controls microglial process ramification and surveillance[21]. Our results, however, showed that isoflurane increased rather than decreased microglial process surveillance. Therefore, to determine whether the microglial process surveillance changes were unique to isoflurane administration or represent a broader microglial response to general anesthesia, we also investigated the effects of two other commonly used anesthetics: ketamine/xylazine and urethane. Similar to isoflurane inhalation, systemic administration (intraperitoneal) of either ketamine/xylazine (87.5 mg per kg ketamine and 12.5 mg per kg xylazine) or urethane (1.6 g per kg) increased microglial process surveillance (Fig. 1h,i). Thus, multiple classes of general anesthetics can enhance microglial process surveillance relative to the awake state. Our results suggest that the awake condition may represent a constrained state of microglia in surveying the brain parenchyma.

To further delineate the potential function of microglial process surveillance, we assessed two events: (1) microglial process chemotaxis toward laser injury and (2) microglial process interaction with neuronal dendrites. We found that the velocity of microglial process chemotaxis in response to laser burn was significantly higher under anesthesia than in the awake condition (Supplementary Fig. 4a). Next, we used *Cx3cr1*$^{GFP/+}$:*Thy1-YFP* mice to examine microglial process interaction with neuronal dendrites in vivo. We found that microglial processes displayed longer contact duration and a larger contact area with dendrites under anesthesia compared to the awake condition (Supplementary Fig. 4b,c). These latter results suggest that increased microglial process surveillance could be translated into enhanced microglia–neuron interaction under anesthesia.

Whisker trimming increases microglial process surveillance in awake mice. Suppressed neuronal activity precedes the increase in microglial process surveillance under general anesthesia, which suggests that neuronal activity might negatively regulate microglial process dynamics. However, general anesthesia also alters metabolism, blood pressure and cardiac output[22]. For these reasons, we additionally employed unilateral whisker trimming as an approach to reduce neuronal activity and to study microglial process dynamics[23]. Whisker trimming is a sensory-deprivation method that suppresses neuronal activity in the contralateral barrel cortex, as demonstrated by calcium imaging in GCaMP6s-expressing cortical neurons (Supplementary Fig. 5a–c; Supplementary Video 3). In response to whisker trimming, microglia in the contralateral barrel cortex began to increase their process area and survey a greater territory of the barrel cortex, similarly to responses we observed for general anesthesia (Fig. 2a,b; Supplementary Video 4). Moreover, the latency for microglia to increase their surveillance after whisker trimming had a similar delayed-onset time course compared to anesthesia (Supplementary Fig. 5d,e). Sensory deprivation only increased process surveillance in microglia of the contralateral barrel cortex, with no effect observed for microglia of the ipsilateral barrel cortex (Fig. 2c,d). Therefore, these results demonstrate that reductions in region-specific sensory input selectively and negatively regulate microglial process surveillance.

Our whisker trimming experiments further substantiate the observation that reduced neuronal activity enhances microglial process surveillance. To determine whether sensory deprivation and general anesthesia increase microglial process surveillance through unique or shared mechanisms, we determined whether their combination had an additive effect on microglial surveillance. To this end, we performed unilateral whisker trimming followed by isoflurane inhalation after an additional 30 min. We found that whisker trimming increased microglial process surveillance, but the addition of isoflurane anesthesia did not further increase process surveillance (Fig. 2e,f). Thus, whisker trimming and isoflurane anesthesia do not have additive effects on microglial process surveillance, which suggests that they may share a similar mechanism for triggering an increase in microglial process dynamics.

Both pharmacological and optogenetic inhibition of neuronal network activity increase microglial process surveillance in awake mice. Results from the general anesthesia and sensory-deprivation paradigms indicate that neuronal activity regulates microglial process dynamics. To directly test this idea, we manipulated cortical network activity through pharmacological and optogenetic approaches and then examined microglial process surveillance. We used an intracerebral catheter and applied a potent and selective agonist for $GABA_A$ receptors, muscimol (870 µM, 10 µl), to suppress neuronal network activity in the somatosensory cortex (Fig. 3a). Indeed, we found that muscimol application in awake mice reduced neuronal calcium activity in the somatosensory cortex (Supplementary Fig. 6; Supplementary Video 5). Coincident with the reduction in neuronal calcium activity, microglia increased their process surveillance (Fig. 3a,c; Supplementary Video 6). By contrast, intracerebral application of artificial cerebrospinal fluid (ACSF) did not alter microglial process surveillance (Fig. 3b). Similarly, we found that microglial surveillance increased after intracerebral application of TTX (10 µM) to inhibit neuronal firing in the awake animal (Supplementary Fig. 7). Thus, pharmacological inhibition

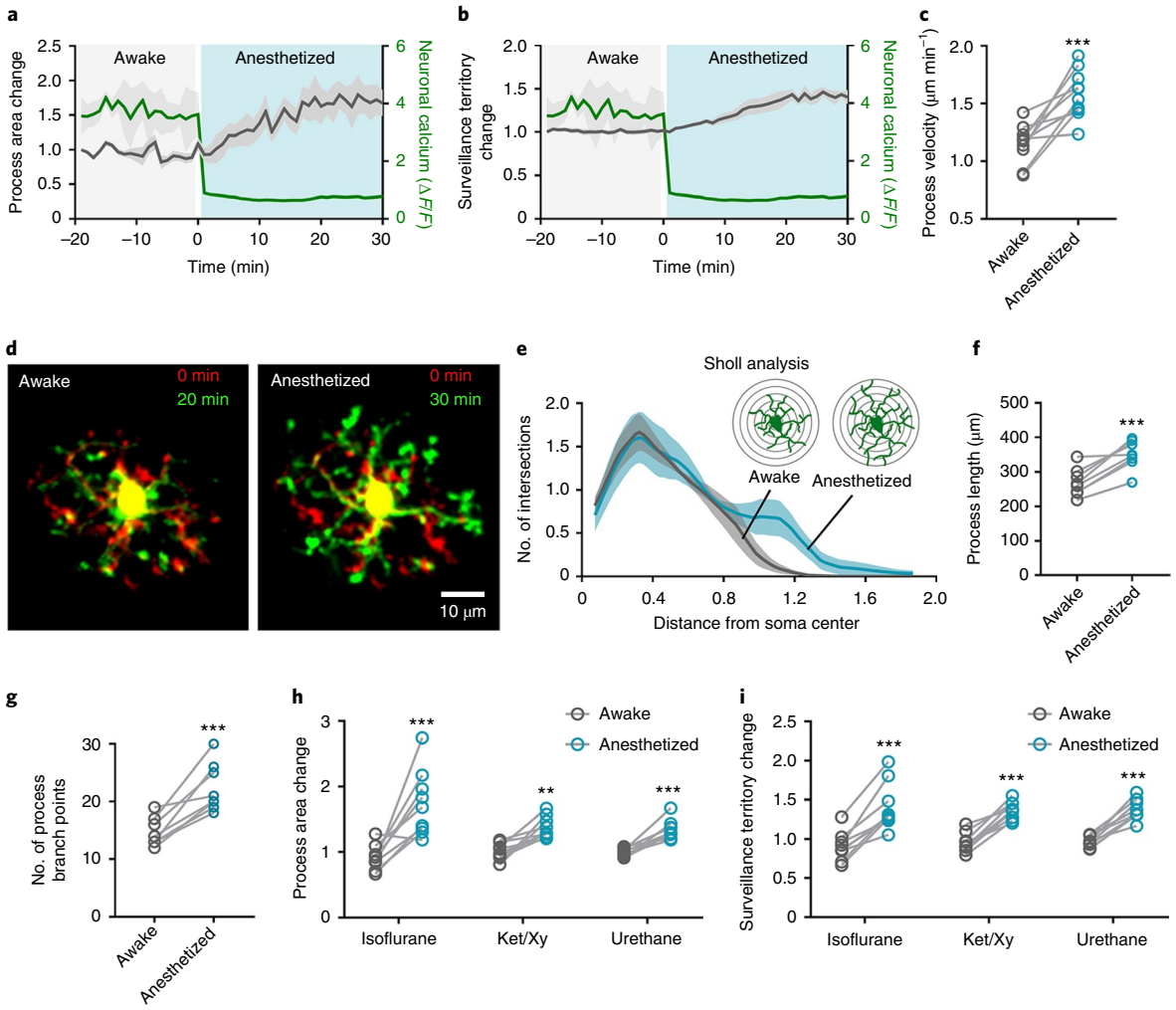

Fig. 1 | Microglial process surveillance is increased after general anesthesia. a,**b**, Time-lapse changes in microglial process area (**a**) and surveillance territory (**b**) overlaid with corresponding changes in neuronal calcium activity as the animal transitions from an awake to an anesthetized state. Isoflurane was used for anesthesia induction and maintenance (**a**–**g**). **c**, Process velocity changes under awake and anesthetized conditions ($n = 12$ cells per 3 mice; $P < 0.0001$, $t(11) = 6.031$). **d**, Representative images of microglial morphology changes over a 20-min period during the awake condition and under isoflurane anesthesia. **e**–**g**, Sholl analysis of microglial morphology (**e**), along with changes in microglial process length (**f**) ($P = 0.0002$, $t(8) = 6.302$) and process branch points (**g**) ($P = 0.0003$, $t(8) = 6.22$) before and after anesthesia. **h**,**i**, Microglial process area (**h**) (isoflurane: $P = 0.0003$, $t(8) = 4.647$; ketamine/xylazine (Ket/Xy): $P = 0.0011$, $t(8) = 4.969$; urethane: $P = 0.0001$, $t(8) = 6.763$) and surveillance territory (**i**) (isoflurane: $P = 0.0001$, $t(8) = 7.093$; Ket/Xy: $P = 0.0001$, $t(8) = 9.134$; urethane: $P = 0.0001$, $t(8) = 9.102$) changes induced by different anesthetic agents: isoflurane, ketamine/xylazine and urethane compared with the awake baseline period. $N = 9$ cells per 3 mice for each group; $^{**}P \leq 0.01$, $^{***}P \leq 0.001$, paired t-test (two-tailed), unless otherwise indicated. For **a**, **b** and **e**, trend lines represent the mean ± s.e.m. For **d**, experiments were repeated three times independently with similar results obtained.

of local neuronal network activity in the cortex is able to recapitulate the changes in microglial process dynamics induced by general anesthesia or whisker trimming.

Next, we employed an optogenetic strategy to suppress neuronal activity. Channelrhodopsin 2 (ChR2) was expressed in VGAT-positive GABAergic neuron populations using *VGAT-ChR2* transgenic mice. Optogenetic activation of GABAergic cell populations in this transgenic line has previously been shown to suppress neuronal network activity[24]. Proper ChR2 expression and function in VGAT-positive interneurons was confirmed in our experiments by whole-cell patch-clamp recording in acute brain slices (Fig. 4a,b; Supplementary Fig. 8a,b). We found that in awake mice, activation of VGAT-ChR2 by 470-nm blue light (10 Hz, 10 min) increased microglial process surveillance (Fig. 4c,d; Supplementary Video 7; Fig. 8c,d). Building on findings obtained from the general anesthesia experiments (Supplementary Fig. 3), transient and reversible network inhibition via optogenetic methods triggered a prolonged increase in microglial surveillance that was sustained for at least 20 min (Supplementary Fig. 8c,d). Together, these results demonstrate that inhibition of local cortical network activity by pharmacological or optogenetic means can trigger an increase in microglial process surveillance in awake mice.

NE signaling regulates microglial process surveillance in awake mice. Next, we investigated the molecular mechanisms underlying the observed increase in microglial process surveillance following neuronal activity suppression. To date, the ATP/ADP-sensing $P2Y_{12}$ receptor has been shown to regulate microglial process extension in a variety of contexts[14,20,25]. To test whether $P2Y_{12}$ receptor signaling mediates the observed increase in microglial process surveillance, we imaged process surveillance in $P2Y_{12}$ receptor-deficient mice (*Cx3cr1*$^{GFP/+}$:*P2y12*$^{-/-}$). Surprisingly, we found that in *P2y12*$^{-/-}$ mice,

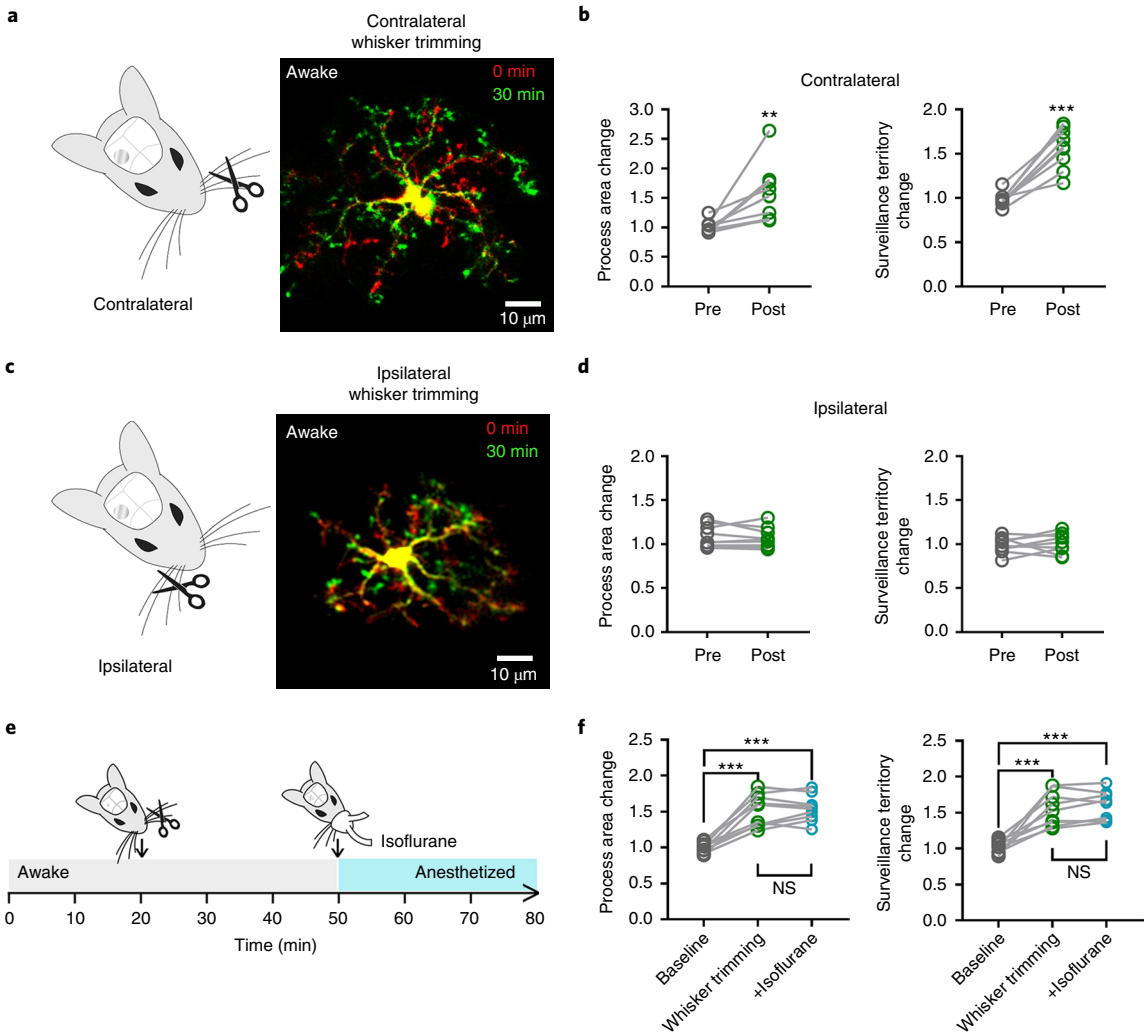

Fig. 2 | Whisker trimming increases microglial process surveillance in the barrel cortex of awake mice. a, Microglial morphology in the contralateral barrel cortex before (0 min) and 30 min after whisker trimming in awake mice. **b**, Microglial process area and surveillance territory increases after trimming the contralateral whiskers (area: $P = 0.0079$, $t(8) = 3.512$; territory: $P = 0.0001$, $t(8) = 8.152$). **c**, Microglial morphology in the ipsilateral barrel cortex before (0 min) and 30 min after whisker trimming in awake mice. **d**, No changes in microglial process area and surveillance territory are observed after trimming the ipsilateral whiskers (area: $P = 0.5439$, $t(8) = 0.63337$; territory: $P = 0.5086$, $t(8) = 0.6919$). **e**, Experimental paradigm: microglial process dynamics were studied in the awake mouse at baseline before trimming the contralateral whiskers 20 min later. Isoflurane was then introduced 30 min after whisker trimming. **f**, Microglial process area and surveillance increases in the contralateral barrel cortex following trimming, but do not show an additional increase when isoflurane is later administered (area: whisker trimming versus baseline, $P < 0.0001$, $t(8) = 7.34$; +isoflurane versus baseline, $P < 0.0001$, $t(8) = 9.153$; whisker trimming versus +isoflurane, $P = 0.624$, $t(8) = 0.5097$; territory: whisker trimming versus baseline, $P = 0.0004$, $t(8) = 5.89$; +isoflurane versus baseline, $P = 0.0002$, $t(8) = 6.639$; whisker trimming versus +isoflurane, $P = 0.2184$, $t(8) = 1.336$). $N = 9$ cells per 3 mice for each group; NS, not significant, $^{**}P \leq 0.01$, $^{***}P \leq 0.001$, paired *t*-test (two-tailed). For **a** and **c**, experiments were repeated three times independently with similar results obtained.

isoflurane anesthesia still increased microglial process surveillance (Fig. 5a,b). Therefore, unlike injury or hyperactivity-induced microglial process extension[20,26], the observed increase in microglial surveillance following isoflurane is not regulated by $P2Y_{12}$ signaling. Fractalkine signaling and its receptor CX_3CR1 are reported to promote microglial process dynamics and microglia–neuron interactions[27]. Therefore, we used *Cx3cr1*$^{-/-}$ (*Cx3cr1*$^{GFP/GFP}$) mice to test whether CX_3CR1 contributes to the increased anesthesia-induced microglial surveillance. We found that isoflurane anesthesia in *Cx3cr1*$^{-/-}$ mice similarly increased microglial process surveillance (Fig. 5c,d), which suggests that fractalkine signaling is not involved in increasing microglial surveillance following anesthesia.

Previous studies have found that primary neurotransmitters such as glutamate and GABA cannot directly induce microglial process chemotaxis[20,28]. For these reasons, we focused instead on investigating whether the neurotransmitters acetylcholine, dopamine, NE and serotonin affected microglial process dynamics. These neurotransmitters were specifically studied because their activity is significantly decreased by general anesthesia[29]. We intracerebrally applied each neurotransmitter during isoflurane inhalation (Fig. 5e). Interestingly, we found that NE (3 mM, 10 µl) application, but not acetylcholine (5 mM, 10 µl), dopamine (1 mM, 10 µl) or serotonin (5 mM, 10 µl), prevented the increase in microglial process surveillance induced by isoflurane anesthesia (Fig. 5f). These results suggest that reduced NE signaling in the anesthetized condition selectively increases microglial process surveillance.

We further studied the regulation of microglial process surveillance by NE during whisker trimming and optogenetic inhibition

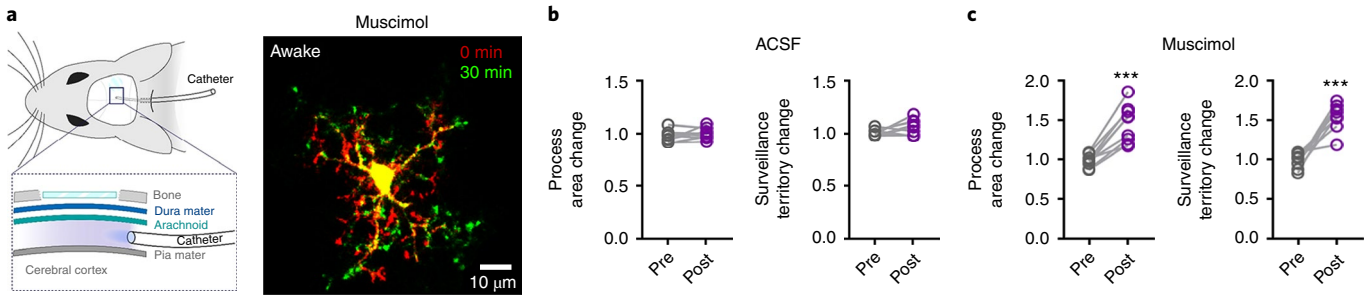

Fig. 3 | Intracerebral application of muscimol increases microglial process surveillance. a, Left: schematic of placement of a drug infusion catheter in the subarachnoid space adjacent to the area of cranial window imaging. Right: images of microglia before (0 min) and 30 min after intracerebral administration of muscimol (870 μM). **b**,**c**, Changes in microglial process area and surveillance territory before and after administration of ACSF (**b**) (area: $P = 0.2681$, $t(8) = 1.19$; territory: $P = 0.0911$, $t(8) = 1.92$) or muscimol (**c**) (area: $P < 0.0001$, $t(8) = 7.338$; territory: $P < 0.0001$, $t(8) = 7.386$). $N = 9$ cells per 3 mice for each group; $^{***}P \leq 0.001$, paired t-test (two-tailed). For **a**, experiments were repeated three times independently with similar results obtained.

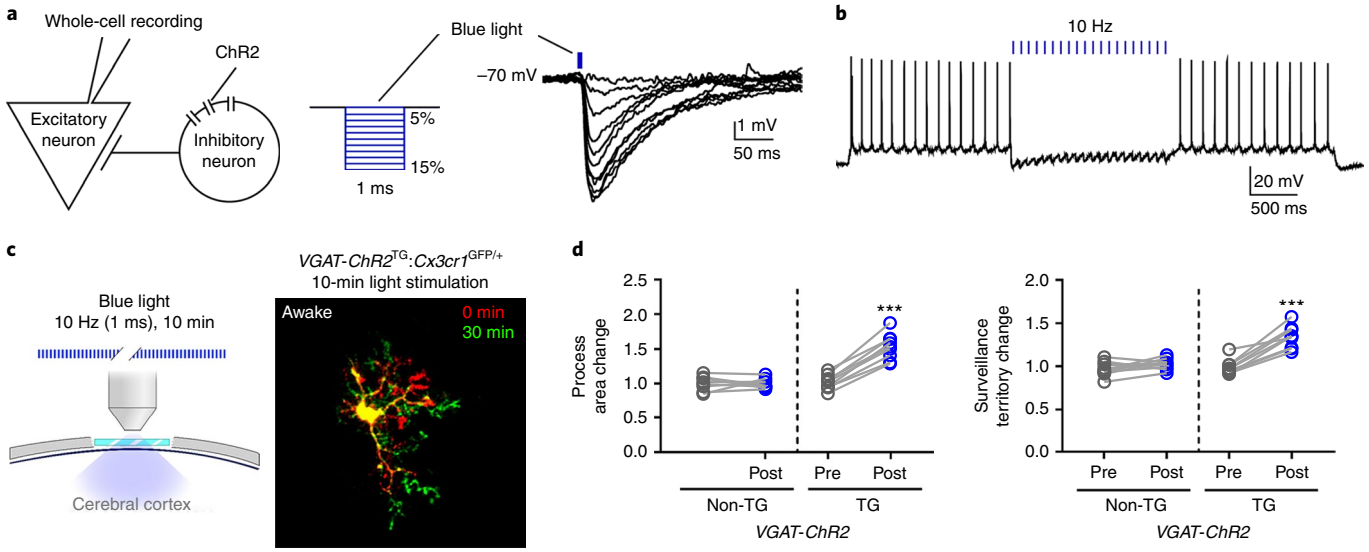

Fig. 4 | Optogenetic suppression of neuronal activity through VGAT-ChR2-mediated inhibition increases microglial process surveillance. a, Left: whole-cell recording of an excitatory neuron (identified by firing pattern and morphology) adjacent to an inhibitory interneuron expressing ChR2 in a brain slice. Right: a blue light pulse (1 ms, 470 nm) induces intensity-dependent (5–15%) membrane hyperpolarization in the neuron, recorded in current-clamp mode. **b**, A 10 Hz train of blue light pulses inhibits local excitatory neuron firing in real time. **c**, Left: in vivo experimental paradigm for inducing on-demand inhibition in the somatosensory cortex (470 nm light, 10 Hz train, 1 ms pulse, 10 min). Right: representative image of microglial morphology before (0 min) and after 10 min of light stimulation. **d**, Changes in microglial process area (non-TG: $P = 0.7144$, $t(8) = 0.3793$; TG: $P < 0.0001$, $t(8) = 12.67$) and surveillance territory (non-TG: $P = 0.1140$, $t(8) = 1.774$; TG: $P < 0.0001$, $t(8) = 8.051$) before and after light stimulation in animals expressing the *VGAT-ChR2* transgene (TG) and in their non-transgenic sibling littermates (non-TG). $N = 9$ cells per 3 mice for each group; $^{***}P \leq 0.001$, paired t-test (two-tailed). For **a**–**c**, experiments were repeated three times independently with similar results obtained.

(Fig. 6). Intracerebral NE administration, but not ACSF administration, prevented the increase in microglial process surveillance induced by contralateral whisker trimming (Fig. 6a–c). Intracerebral NE administration also prevented the increase in microglial process surveillance induced by optogenetic inhibition (Fig. 6d–f).

β_2-adrenergic receptors control microglial process surveillance in awake mice. Microglia are known to express high levels of β_2-adrenergic receptors[30]. Their activation induces microglial process retraction in brain slices[31]. Using RNAscope in situ hybridization, we indeed found that most IBA1-positive microglia (97.6%) colocalized with β_2-adrenergic receptor (*Adrb2*) mRNA (Supplementary Fig. 9). To explore whether adrenergic receptors control microglial process activity in awake mice, we examined the effects of β-adrenergic receptor antagonists on microglial dynamics (Fig. 7a–c). Interestingly, both propranolol (300 μM, 10 μl; Fig. 7b), a high-affinity anatagonist of β_1- and β_2-receptors, and the highly selective β_2-receptor antagonist ICI 118,551 (30 μM, 10 μl; Fig. 7c) induced an increase in microglial process surveillance in awake mice. In addition, an intracerebral injection of TTX (50 μM) followed by application of ICI 118,551 (10 μM) 30 min later did not further increase microglial surveillance (Supplementary Fig. 7). Thus, inhibition of β_2-adrenergic receptors can increase microglial process dynamics.

Cortical NE tone is largely generated by noradrenergic neurons in the LC[32], which project into the somatosensory cortex (Fig. 7d; Supplementary Video 8). Microglial processes are in close proximity to noradrenergic axons, as shown by labeling with adeno-associated viruses (AAVs; a combination of AAV.rTH.Cre and AAV.FLEX.tdTomato; Fig. 7d). To directly study the effect of NE signaling on

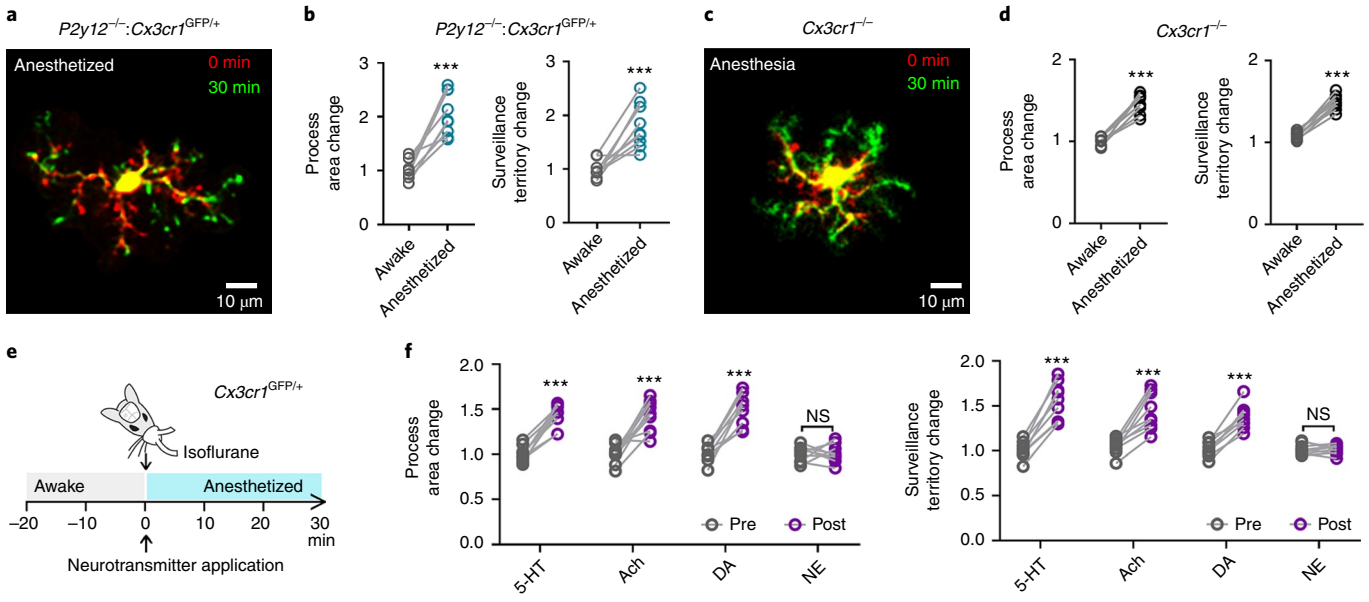

Fig. 5 | NE signaling, but not P2Y$_{12}$ or CX$_3$CR1 signaling, contributes to microglial surveillance increases. a, Representative image of *P2y12*$^{-/-}$ microglial morphology before (0 min) and 30 min after isoflurane anesthesia. **b**, The previously reported increases in microglial process area and surveillance territory following isoflurane anesthesia are not prevented by *P2y12*$^{-/-}$ (area: $P < 0.0001$, $t(8) = 7.4$; territory: $P = 0.0007$, $t(8) = 5.306$). **c**, Representative image of *Cx3cr1*$^{-/-}$ microglial morphology before (0 min) and 30 min after isoflurane anesthesia. **d**, The previously reported increases in microglial process area and surveillance territory following isoflurane anesthesia are not prevented by *Cx3cr1*$^{-/-}$ (area: $P < 0.0001$, $t(8) = 10.13$; territory: $P < 0.0001$, $t(8) = 13.76$). **e**, Experimental paradigm used to test the effects of different candidate neurotransmitters on microglial process dynamics during isoflurane anesthesia. **f**, Changes in microglial process area and surveillance territory in response to isoflurane anesthesia are not affected by intracerebral administration of acetylcholine (Ach; area: $P = 0.0005$, $t(8) = 5.584$; territory: $P = 0.0003$, $t(8) = 6.084$), dopamine (DA; area: $P < 0.0001$, $t(8) = 7.538$; territory: $P < 0.0001$, $t(8) = 8.586$) or serotonin (5-HT; area: $P < 0.0001$, $t(8) = 8.995$; territory: $P < 0.0001$, $t(8) = 9.944$). However, intracerebral administration of NE prevents the observed increases in microglial process area and surveillance territory following isoflurane anesthesia (area: $P = 0.9346$, $t(8) = 0.08465$; territory: $P = 0.7332$, $t(8) = 0.3531$). $N = 9$ cells per 3 mice for each group; $^{***}P \leq 0.001$, paired *t*-test (two-tailed). For **a** and **c**, experiments were repeated three times independently with similar results obtained.

microglia, we used a chemogenetic approach to selectively suppress noradrenergic neurons in the LC by activating Gi-DREADD, which decreases cAMP levels and generally reduces neuronal firing rates. A Gi-DREADD-*loxP*-flanked mouse (R26-LSL-Gi-DREADD) was bred with the *Cx3cr1*$^{GFP/+}$ line. Expression of the Gi-DREADD receptor was confined to the LC through a targeted AAV-Cre injection (AAV9.rTH.PI.Cre.SV40) (Fig. 7e). In awake mice, the systemic application of the DREADD ligand clozapine-*N*-oxide (CNO; 5 mg per kg, intraperitoneally) increased microglial process surveillance in the somatosensory cortex in Gi-DREADD-expressing mice but not in their control littermates (Fig. 7f–h). We confirmed that CNO reduced the firing rate of Gi-DREADD-expressing noradrenergic neurons in the LC using acute brain slices (Supplementary Fig. 10a–d). In addition, to test potential off-target effects of CNO, we applied CNO in anesthetized Gi-DREADD mice and examined microglial process dynamics. We found that CNO did not further increase microglial surveillance in the anesthetized state (Supplementary Fig. 10e). Therefore, our results suggest that CNO targets Gi-DREADD to reduce endogenous NE release and subsequently increase microglial process surveillance.

To better access and mechanistically study the LC–cortex circuitry, we performed several experiments in acute cortical slices. In slices, noradrenergic projections were well preserved (Supplementary Fig. 11a), but their connections to noradrenergic somata were severed during slice preparation (see Methods). Unlike the in vivo context (Supplementary Video 2), neuronal network activity was weak in cortical slices (Supplementary Fig. 11b,c; Supplementary Video 9). Bath application of a moderate dose of glutamate (50 μM) increased neuronal activity in cortical slices (Supplementary Fig. 11b,c; Supplementary Video 9), which resulted in reduced microglial surveillance (Fig. 8a). We further found that the β_2-adrenergic receptor antagonist ICI 118,551 (10 μM) blocked the glutamate-induced decreases in microglial surveillance (Fig. 8b). Next, to test the direct effect of NE on microglial dynamics in cortical brain slices, we applied exogenous NE or chemogenetically induced endogenous NE release. Indeed, exogenous application of NE (30 μM) inhibited microglial process surveillance in cortical slices; this effect was abolished by ICI 118,551 (10 μM) (Fig. 8c). The application of ICI 118,551 (10 μM) alone did not affect microglial process surveillance, presumably due to the low activity of NE-releasing axons in brain slices (Fig. 8c). In slices prepared from mice with viral-induced expression of Gq-DREADD in LC adrenergic neurons and their projections, CNO was confirmed to increase neuronal firing (Fig. 8d,e). In addition, activation of noradrenergic terminals by CNO reduced microglial process surveillance (Fig. 8f). Therefore, our results suggest that local neuronal activity affects NE signaling, which is sufficient to regulate microglial process surveillance, even in the absence of LC somata.

Together, both β_2-adrenergic receptor antagonism and chemogenetic inhibition of NE release can increase microglial process surveillance in awake mice. Inhibiting NE signaling therefore mirrors the effects of general anesthesia, sensory deprivation and optogenetic inhibition on microglial process surveillance. Overall, our results demonstrate that reduced NE signaling establishes a permissive microenvironment for enhanced microglial process surveillance. Meanwhile, tonic NE levels in the awake animal repress process surveillance and maintain a highly constrained microglial surveying state (Supplementary Fig. 12).

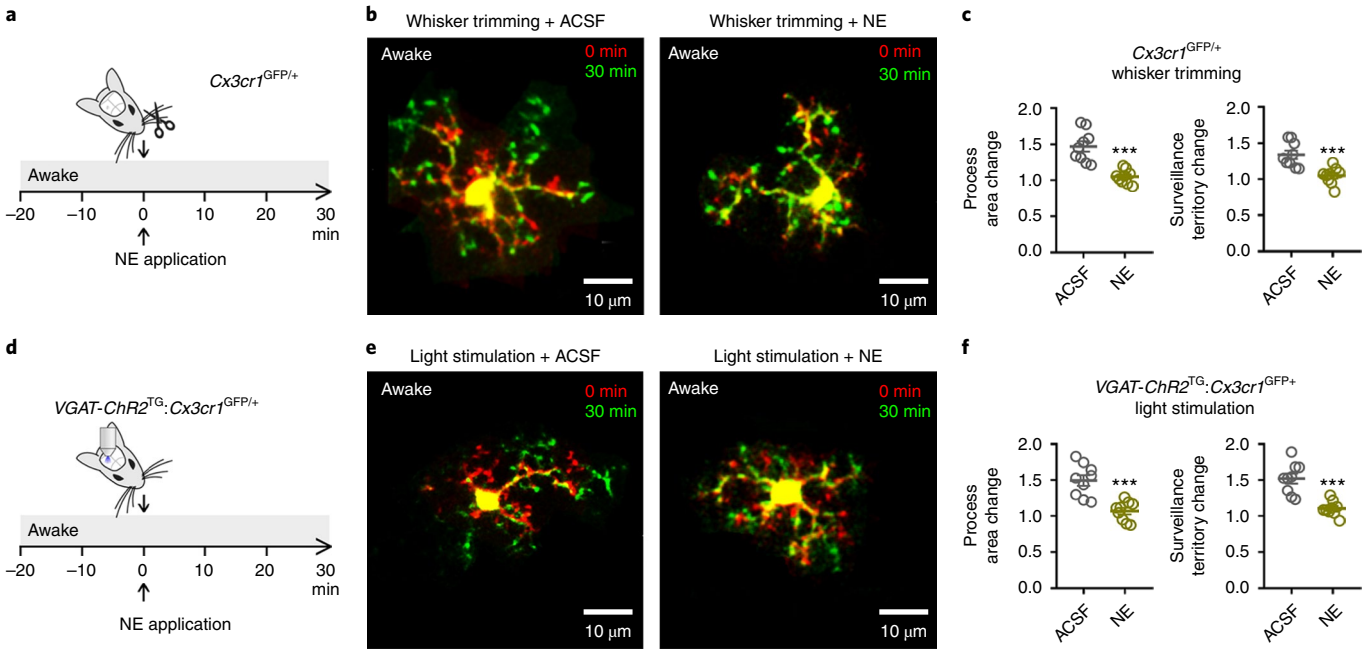

Fig. 6 | NE administration before whisker trimming or optogenetic inhibition prevents the increase in microglial process surveillance. a, Experimental paradigm: NE (or ACSF control solution) was administered intracerebrally immediately before contralateral whisker trimming. **b**, Representative images of microglial morphology before (0 min) and 30 min after whisker trimming, with either ACSF or NE applied. **c**, NE, but not ACSF, prevents changes in microglial process area (ACSF: 1.473 ± 0.072; NE: 1.048 ± 0.030) and surveillance territory (ACSF: 1.341 ± 0.058; NE: 1.038 ± 0.037) induced by contralateral whisker trimming (area: $P < 0.0001$, $t(16) = 5.432$; territory: $P = 0.0005$, $t(16) = 4.395$). **d**, Experimental paradigm: NE (or ACSF control solution) was administered intracerebrally immediately before optogenetic stimulation of *VGAT-ChR2* transgenic mice. **e**, Representative images of microglial morphology before (0 min) and 30 min after optogenetic inhibition, with either ACSF of NE applied immediately before light stimulation. **f**, NE, but not ACSF, also prevents changes in microglial process area (ACSF: 1.496 ± 0.075; NE: 1.060 ± 0.045) and surveillance territory (ACSF: 1.523 ± 0.070; NE: 1.106 ± 0.033) induced by optogenetic inhibition (area: $P = 0.0001$, $t(16) = 5$; territory: $P < 0.0001$, $t(16) = 5.334$). $N = 9$ cells per 3 mice for each group; $^{***}P \leq 0.001$, unpaired *t*-test (two-tailed). For **b** and **e**, experiments were repeated three times independently with similar results obtained.

Discussion

Microglia are the immune surveilling cells of the brain that shape neuronal circuitry in both health and disease[6]. Multiple studies have demonstrated that the interactions between microglial processes and neuronal elements play a critical role in maintaining brain homeostasis[9,18]. However, microglial process dynamics in vivo have been studied predominantly under anesthesia. Moreover, it is unclear whether neuronal network activity under awake conditions drive distinct microglial dynamics. Here, using in vivo imaging in awake mice, we showed that general anesthesia, sensory deprivation and optogenetic inhibition of local neuronal activity dramatically increases microglial process surveillance. We also pinpointed the underlying mechanism involved in the increased process surveillance, which arises from a reduction in NE signaling to microglial β_2-adrenergic receptors. These results demonstrate that neuronal network activity inhibits microglial process dynamics through tonic NE signaling in awake mice.

Neuronal activity dictates microglial process dynamics. Prior studies of microglial imaging under anesthesia and of brain slices found that microglial process dynamics seem to follow neuronal activity patterns. Increased neuronal activity after bicuculline application, a $GABA_A$ receptor antagonist, enhances microglial process sampling[13]. In addition, neuronal hyperactivity triggered by NMDA receptor activation induces microglial process extension toward neuronal cell bodies and dendrites[20,26]. Consistently, acute seizures increase microglial process dynamics and process convergence toward neuronal elements[20]. During neuronal hyperactivity (for example, under seizure conditions), microglia can sense ATP release via the $P2Y_{12}$ receptor and extend and converge their process toward an ATP source[20,26].

We expected that microglia in the awake animal would display more pronounced motility. Surprisingly, we found opposite results, showing that microglia exhibit less process surveillance in the awake condition than under general anesthesia. Consistently, introducing sensory deprivation or increased GABAergic network inhibition in awake animals resulted in similar increases in microglial process dynamics. Supporting this novel observation, a recent study reported that monocular deprivation induced greater microglial process ramification in the contralateral visual cortex[33]. Together, our results reveal that neuronal activity negatively regulates microglial surveillance in awake mice. Therefore, in awake mice, microglial process dynamics are kept in a relatively constrained state.

Our results, in combination with previous studies that used general anesthesia, suggest that microglial process dynamics are not linearly dependent on neuronal activity (that is, increasing neuronal activity increases microglial process dynamics). Rather, microglial dynamics follows a U-shaped curve of regulation; that is, either increasing or decreasing neuronal activity relative to the awake state can increase microglial process dynamics. While microglial extension and convergence during hyperactivity or acute injury has been demonstrated through an ADP/ATP and $P2Y_{12}$-receptor-dependent mechanism, we show here that a reduction in NE tone and β_2-adrenergic activation (due to suppressed neuronal activity) results in microglial extension and territory surveillance. Although our results ruled out the contribution of $P2Y_{12}$ receptor signaling in the increased territory surveillance, other studies have demonstrated that microglial $P12Y_{12}$ and β_2-adrenergic receptors control

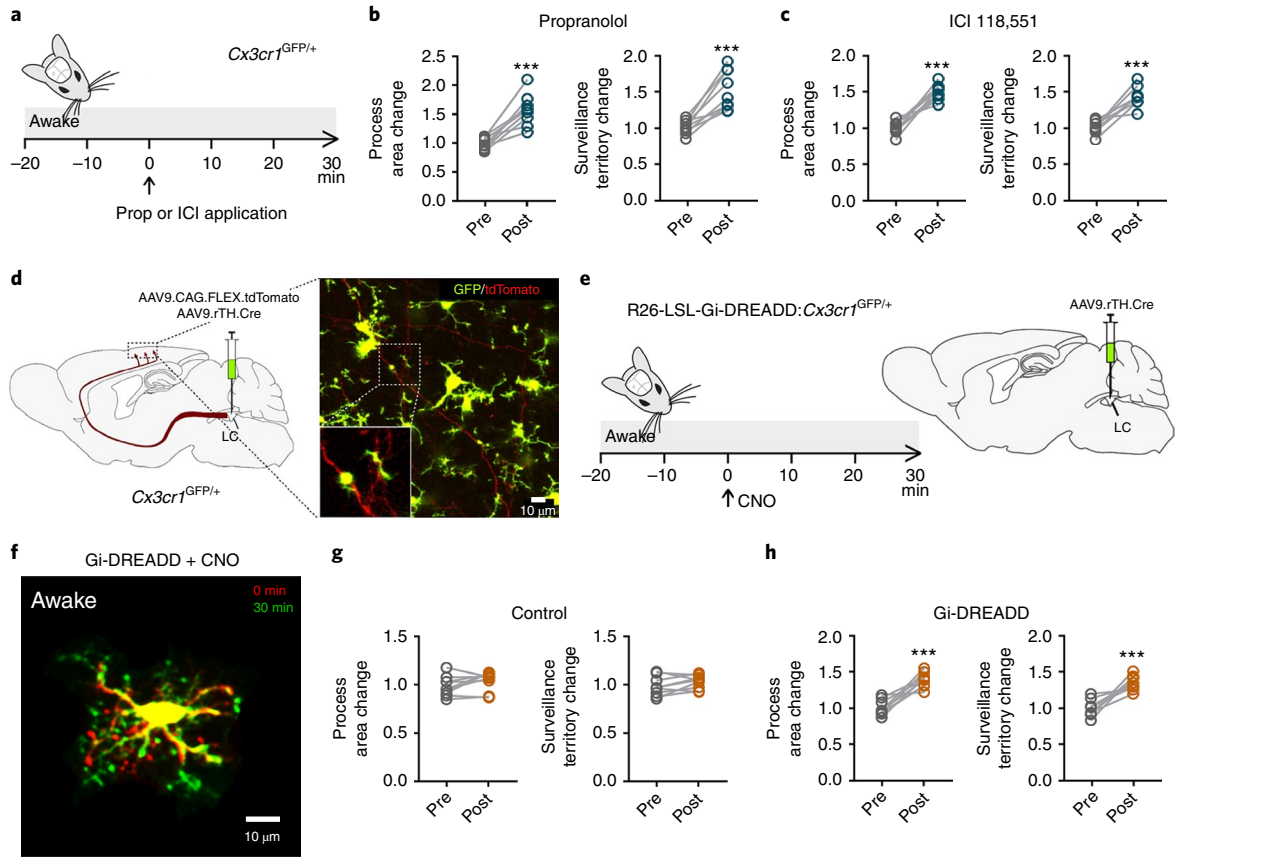

Fig. 7 | Blocking adrenergic receptors or lowering endogenous NE signaling increases microglial process surveillance. a, Experimental paradigm: the β_1/β_2-adrenergic receptor antagonist propranolol (Prop) or the β_2-receptor antagonist ICI 118,551 (ICI) was administered intracerebrally in awake mice. **b**,**c**, Both propranolol (**b**) (area: $P=0.0002$, $t(8)=6.331$; territory: $P=0.0003$, $t(8)=6.204$) and ICI 118,551 (**c**) (area: $P<0.0001$, $t(8)=9.024$; territory: $P=0.0001$, $t(8)=7.109$) infusion in awake mice trigger an increase in microglial process area and territory surveillance. **d**, Left: to determine the extent of noradrenergic innervation in the somatosensory cortex by LC neurons, td-Tomato expression was induced selectively in LC neurons using a specific Cre recombination strategy in *Cx3cr1*$^{GFP/+}$ mice. Right: the fluorescent micrograph shows heavy noradrenergic innervation of the somatosensory cortex by LC projections. **e**, Experimental paradigm: the DREADD receptor agonist CNO was administered (intraperitoneally) to Gi-DREADD mice and control sibling littermates. **f**, Representative image of microglial morphology before (0 min) and 30 min after CNO administration in a Gi-DREADD mouse. **g**,**h**, CNO administration in control mice (**g**) does not alter microglial process area or territory surveillance (area: $P=0.1193$, $t(8)=1.744$; territory: $P=0.1326$, $t(8)=1.674$), while CNO administration in Gi-DREADD mice (**h**) increases microglial process area and territory surveillance (area: $P=0.0001$, $t(8)=6.815$; territory: $P=0.0005$, $t(8)=5.67$). $N=9$ cells per 3 mice for each group; $^{***}P\leq0.001$, paired *t*-test (two-tailed). For **d** and **f**, experiments were repeated three times independently with similar results obtained.

microglial process motility in vitro through interacting mechanisms[31]. Overall, our study demonstrates that microglial dynamics are highly attuned to changes in the local microenvironment, but follow a U-shape style of regulation rather than linear activity-dependent regulation.

Tonic NE and microglial process dynamics. Here, we demonstrated that tonic NE signaling selectively regulates microglial process surveillance in vivo, which is based on several lines of evidence. First, of the four potential neuromodulators tested (acetylcholine, dopamine, NE and serotonin), only NE prevented anesthesia-induced microglial process extension. Second, exogenous NE also prevented the increase in microglial process surveillance induced by whisker trimming and optogenetic inhibition. Finally, pharmacological inhibition of microglial β_2-adrenergic receptors and chemogenetic inhibition of LC noradrenergic neurons increased microglial process surveillance in awake mice. LC noradrenergic neurons are the exclusive source of NE in the cortex[34]. Indeed, we showed that there are abundant LC projections in the somatosensory cortex, consistent with the reported ~1.2 million axon varicosities per LC neuron[35]. Additionally, a wealth of adrenergic receptors are expressed in neurons and glia[36]. Among them, the β_2-adrenergic receptor is highly enriched in microglia compared with other cell types[30]. Previous studies have also shown that microglial β_2-adrenergic receptors are critical for microglial motility, migration, phagocytosis, proliferation and inflammatory responses[36]. Our study corroborates the importance of noradrenergic regulation of microglia function by providing evidence that tonic NE inhibits microglial process surveillance via β_2-adrenergic receptors in awake mice.

While microglia represent an enriched cell population for functional β_2-adrenergic receptor expression[30], the downstream signaling cascades that mediate β_2-receptor-dependent process motility and surveillance are still undefined in microglia. It is known that the β_2-adrenergic receptor is coupled to Gs protein signaling. Thus, inhibition of microglial β_2-receptors should reduce cyclic AMP production, based on canonical Gs signaling[37]. Similarly, the Gi-coupled $P2Y_{12}$ receptor, which also alters cAMP levels, induces microglial process chemotaxis, while the Gs-coupled A_{2A} receptor mediates microglial process retraction[38]. Therefore, it seems that the intracellular cAMP level is important in regulating microglial process surveillance. Indeed, a very recent study demonstrated that

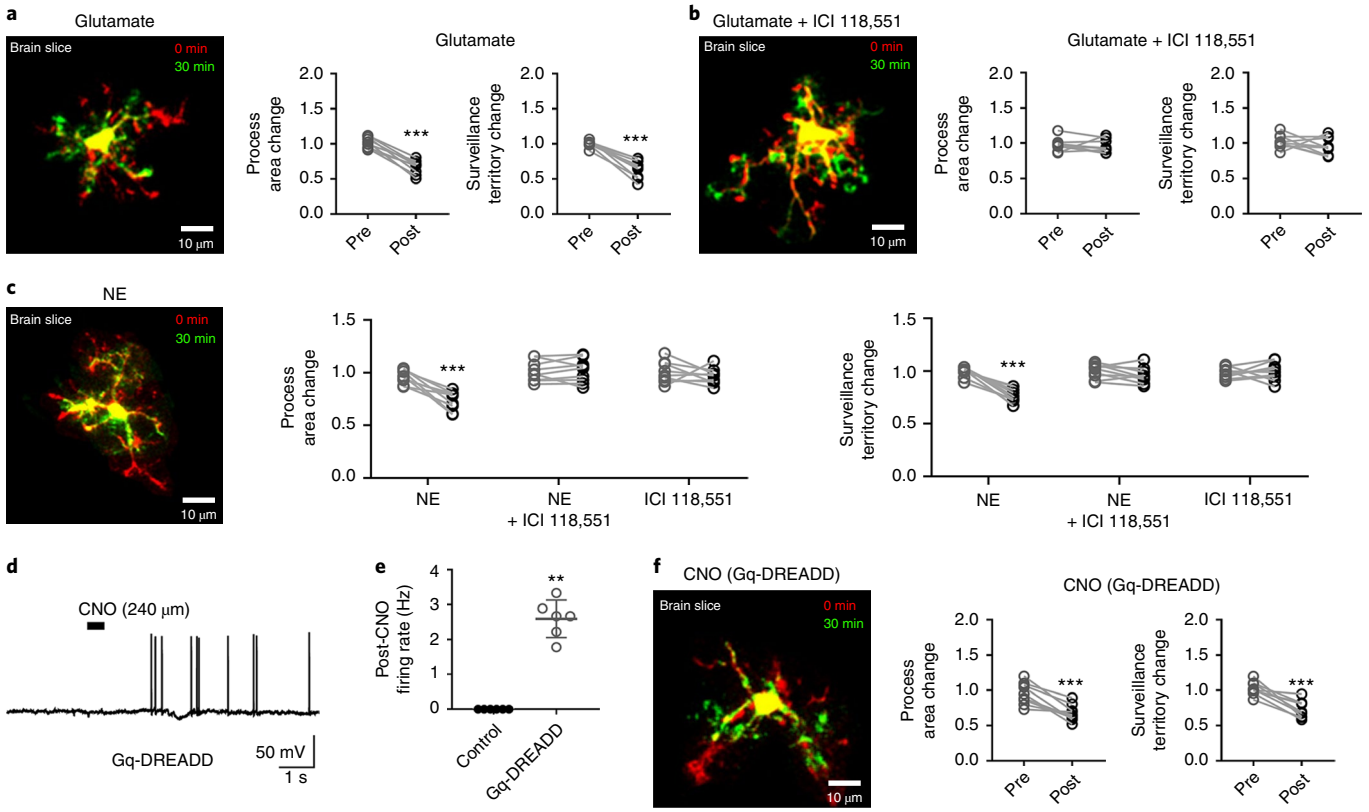

Fig. 8 | NE decreases microglial process surveillance in acute brain slices. a,**b**, Microglial morphology changes in acute brain slices before (0 min) and 30 min after bath application of 50 μM glutamate (**a**) (area: $P < 0.0001$, $t(8) = 9.982$; territory: $P < 0.0001$, $t(8) = 8.027$) or 50 μM glutamate with 10 μM ICI 118,551 (**b**) (area: $P = 0.625$, $t(8) = 0.509$; territory: $P = 0.264$, $t(8) = 1.202$). **c**, Microglial morphology changes in acute brain slices before (0 min) and 30 min after bath application of 30 μM NE (area: $P = 0.0003$, $t(8) = 6.127$; territory: $P < 0.0001$, $t(8) = 8.932$), 30 μM NE with 10 μM ICI 118,551 (area: $P = 0.859$, $t(8) = 0.183$; territory: $P = 0.137$, $t(8) = 1.654$) or 10 μM ICI 118,551 (area: $P = 0.420$, $t(8) = 0.850$; territory: $P = 0.672$, $t(8) = 0.440$). **d**, After a delay associated with CNO bath diffusion, Gq-DREADD neurons in the LC display a marked increase in firing frequency. Experiments were repeated three times independently with similar results obtained. **e**, Effects of CNO on firing rates are only observed in Gq-DREADD neurons in the LC, but not in control neurons (control: 0; Gq-DREADD: 593 ± 0.219; $P = 0.002$, $t(10) = 11.8$). $N = 6$ cells per 3 mice for each group; $^{**}P < 0.01$, unpaired t-test (two-tailed). **f**, Microglial morphology changes in acute brain slices from mice expressing Gq-DREADD in the LC before (0 min) and 30 min after bath application of CNO (10 μM) (area: $P = 0.0005$, $t(8) = 5.573$; territory: $P = 0.0004$, $t(8) = 5.797$). $N = 9$ cells per 3 mice for each group; $^{***}P < 0.001$, paired t-test (two tailed), unless otherwise indicated. For **a**–**d** and **f**, experiments were repeated three times independently with similar results obtained.

cAMP controls microglial filopodia dynamics[39]. However, future studies of whether and how cAMP levels drive microglial process surveillance in vivo are still needed.

Our findings strike an interesting contrast to recent work investigating the impact of halogenated anesthetics, such as isoflurane, on microglial process dynamics. Tonic activation of the microglial two-pore domain channel THIK-1 was recently shown to control microglial process ramification and surveillance[21]. THIK-1 inhibition via isoflurane reduces microglial process surveillance in hippocampal slices. In contrast, our study indicates that isoflurane increases microglial process dynamics in the cortex of awake mice. This discrepancy could be due to microglial heterogeneity within different brain regions (hippocampus versus cortex), but could also be explained by the expected attenuation of NE tone that occurs when LC projections are severed during brain slice preparation. In brain slices, microglial surveillance is likely to be elevated in the absence of a strong NE tone. Potentially, when microglia are relieved of the dynamic constraints set by NE tone in slices, they are disposed to greater modulation in the microenvironment. In vivo, it is possible that the effects of isoflurane on NE tone serve as a stronger impetus for altering microglial dynamics than the effects of isoflurane on THIK-1 signaling. However, studies directly assessing β_2-adrenergic and THIK-1 receptor signaling on microglial process surveillance will be necessary to clearly understand the conditions and constraints for their functions.

Functional significance of microglial process dynamics regulated by NE tone. Increased microglial process surveillance broadly suggests that there are more interactions between microglia and features of the brain parenchyma, such as neurons and vasculature[7,40,41]. The functional significance of microglial process interaction with neurons is an emerging field of research. Previous studies have indicated that microglial interaction may dampen neuronal hyperactivity[20,42], while other studies have shown that microglial processes increase dendritic spine Ca^{2+} activity[12] and promote new spine formation during brain development and learning[7,11]. Therefore, microglial process surveillance may play a beneficial role in fine-tuning neuronal activity by reducing neuronal activity during seizures[19,20] or by increasing neuronal synchronization during periods of reduced network activity[12]. Calibrating neuronal activity occurs in response to divergent neuromodulatory signals that exist in various brain states. While distinct receptors (that is, $P2Y_{12}$ and β_2) for these divergent neuromodulators have been identified in microglia, many more receptors are likely to exist and may aid in uniquely tuning microglial responses to the environment[3]. Toward this end, emerging tools for studying intracellular signaling mecha-

nisms, such as cAMP levels, in vivo may greatly advance our ability to understand the complex downstream signaling mechanisms that mediate microglial responses to the microenvironment.

LC noradrenergic neurons innervate almost every region of the brain and could therefore have a widespread, potentially uniform, impact on microglial function. Under physiological conditions, NE regulates the sleep–wake cycle in addition to its role in memory and cognition[34]. The loss of LC neurons is an early hallmark of neurodegeneration, as evident in Alzheimer's disease and Parkinson's disease[43]. Meanwhile, chronic stress increases LC neuronal firing rates and brain NE concentrations[44]. Therefore, the relative loss or gain in NE tone under these different pathophysiological contexts could serve as a powerful upstream modulator of microglial function across numerous brain regions. In turn, corresponding changes in microglial surveillance could produce profound consequences for the neuronal network over time in chronic conditions, based on the described roles for microglia in tuning neuronal activity. In addition, NE has been shown to reduce pro-inflammatory gene expression in microglia in various neurological disorders, including stroke, pain and neurodegeneration[36]. In particular, NE can help resolve pathology in mouse models of Alzheimer's disease by promoting microglial phagocytosis of amyloid-β and reducing amyloid-β-triggered inflammation[45,46]. However, microglia are also reported to be inappropriately activated in Alzheimer's disease and mediate early synapse loss[47]. Apart from disease contexts, NE tone is reduced on a daily basis during sleep[48]. It would be interesting to know whether reduced NE tone during sleep may 'disinhibit' microglial motility to allow greater synaptic remodeling to occur during sleep cycles, which might have implications for the consolidation phase of learning and memory. However, we acknowledge that anesthesia and sleep are not mechanistically identical[49], and microglial dynamics during sleep will need to be explored in greater detail in future studies. Additionally, even with training, head-fixed animals can still remain stressed, thus potentially exaggerating the levels of NE in the awake state. Therefore, for normal animals that are awake but not head-fixed, microglial surveillance could be more pronounced than we report here. Nevertheless, future studies are warranted to test the specific role of microglial adrenergic receptor signaling in sleep, memory and neurodegeneration.

In summary, we provide novel insights into microglial process dynamics under awake conditions and their regulation by neuronal activity and NE tone. Our results demonstrate that microglial process dynamics are fundamentally different in awake animals, emphasizing the importance of studying microglia in awake mice to establish the clearest picture for their basal physiology.

Online content

Any methods, additional references, Nature Research reporting summaries, source data, statements of code and data availability and associated accession codes are available at https://doi.org/10.1038/s41593-019-0511-3.

Received: 14 March 2019; Accepted: 11 September 2019;
Published online: 21 October 2019

References

1. Ransohoff, R. M. & Perry, V. H. Microglial physiology: unique stimuli, specialized responses. *Annu. Rev. Immunol.* **27**, 119–145 (2009).
2. Wolf, S. A., Boddeke, H. W. & Kettenmann, H. Microglia in physiology and disease. *Annu. Rev. Physiol.* **79**, 619–643 (2017).
3. Kettenmann, H., Hanisch, U. K., Noda, M. & Verkhratsky, A. Physiology of microglia. *Physiol. Rev.* **91**, 461–553 (2011).
4. Wu, Y., Dissing-Olesen, L., MacVicar, B. A. & Stevens, B. Microglia: dynamic mediators of synapse development and plasticity. *Trends Immunol.* **36**, 605–613 (2015).
5. Eyo, U. B. & Wu, L. J. Bi-directional microglia–neuron communication in the healthy brain. *Neural Plast.* **2013**, 456857 (2013).
6. Salter, M. W. & Stevens, B. Microglia emerge as central players in brain disease. *Nat. Med.* **23**, 1018–1027 (2017).
7. Miyamoto, A. et al. Microglia contact induces synapse formation in developing somatosensory cortex. *Nat. Commun.* **7**, 12540 (2016).
8. Weinhard, L. et al. Microglia remodel synapses by presynaptic trogocytosis and spine head filopodia induction. *Nat. Commun.* **9**, 1228 (2018).
9. Tremblay, M. E., Lowery, R. L. & Majewska, A. K. Microglial interactions with synapses are modulated by visual experience. *PLoS Biol.* **8**, e1000527 (2010).
10. Schafer, D. et al. Microglia sculpt postnatal neural circuits in an activity and complement-dependent manner. *Neuron* **74**, 691–705 (2012).
11. Parkhurst, C. N. et al. Microglia promote learning-dependent synapse formation through brain-derived neurotrophic factor. *Cell* **155**, 1596–1609 (2013).
12. Akiyoshi, R. et al. Microglia enhance synapse activity to promote local network synchronization. *eNeuro* **5**, ENEURO.0088-18.2018 (2018).
13. Nimmerjahn, A., Kirchhoff, F. & Helmchen, F. Resting microglial cells are highly dynamic surveillants of brain parenchyma in vivo. *Science* **308**, 1314–1318 (2005).
14. Davalos, D. et al. ATP mediates rapid microglial response to local brain injury in vivo. *Nat. Neurosci.* **8**, 752–758 (2005).
15. Eyo, U. B. et al. P2Y12R-dependent translocation mechanisms gate the changing microglial landscape. *Cell Rep.* **23**, 959–966 (2018).
16. Haynes, S. E. et al. The $P2Y_{12}$ receptor regulates microglial activation by extracellular nucleotides. *Nat. Neurosci.* **9**, 1512–1519 (2006).
17. Wu, L. J., Vadakkan, K. I. & Zhuo, M. ATP-induced chemotaxis of microglial processes requires P2Y receptor-activated initiation of outward potassium currents. *Glia* **55**, 810–821 (2007).
18. Wake, H., Moorhouse, A. J., Jinno, S., Kohsaka, S. & Nabekura, J. Resting microglia directly monitor the functional state of synapses in vivo and determine the fate of ischemic terminals. *J. Neurosci.* **29**, 3974–3980 (2009).
19. Eyo, U. B. et al. Regulation of physical microglia–neuron interactions by fractalkine signaling after status epilepticus. *eNeuro* **3**, ENEURO.0209-16.2016 (2017).
20. Eyo, U. B. et al. Neuronal hyperactivity recruits microglial processes via neuronal NMDA receptors and microglial P2Y12 receptors after status epilepticus. *J. Neurosci.* **34**, 10528–10540 (2014).
21. Madry, C. et al. Microglial ramification, surveillance, and interleukin-1beta release are regulated by the two-pore domain K(+) channel THIK-1. *Neuron* **97**, 299–312 e296 (2018).
22. Franks, N. P. General anaesthesia: from molecular targets to neuronal pathways of sleep and arousal. *Nat. Rev. Neurosci.* **9**, 370–386 (2008).
23. Petersen, C. C. The functional organization of the barrel cortex. *Neuron* **56**, 339–355 (2007).
24. Zhao, S. et al. Cell type-specific channelrhodopsin-2 transgenic mice for optogenetic dissection of neural circuitry function. *Nat. Methods* **8**, 745–752 (2011).
25. Eyo, U. B., Murugan, M. & Wu, L. J. Microglia–neuron communication in epilepsy. *Glia* **65**, 5–18 (2017).
26. Dissing-Olesen, L. et al. Activation of neuronal NMDA receptors triggers transient ATP-mediated microglial process outgrowth. *J. Neurosci.* **34**, 10511–10527 (2014).
27. Liang, K. J. et al. Regulation of dynamic behavior of retinal microglia by CX3CR1 signaling. *Invest. Ophthalmol. Vis. Sci.* **50**, 4444–4451 (2009).
28. Wu, L. J. & Zhuo, M. Resting microglial motility is independent of synaptic plasticity in mammalian brain. *J. Neurophysiol.* **99**, 2026–2032 (2008).
29. Muller, C. P. et al. The in vivo neurochemistry of the brain during general anesthesia. *J. Neurochem.* **119**, 419–446 (2011).
30. Zhang, Y. et al. An RNA-sequencing transcriptome and splicing database of glia, neurons, and vascular cells of the cerebral cortex. *J. Neurosci.* **34**, 11929–11947 (2014).
31. Gyoneva, S. & Traynelis, S. F. Norepinephrine modulates the motility of resting and activated microglia via different adrenergic receptors. *J. Biol. Chem.* **288**, 15291–15302 (2013).
32. Schwarz, L. A. & Luo, L. Organization of the locus coeruleus–norepinephrine system. *Curr. Biol.* **25**, R1051–R1056 (2015).
33. Sipe, G. O. et al. Microglial P2Y12 is necessary for synaptic plasticity in mouse visual cortex. *Nat. Commun.* **7**, 10905 (2016).
34. Berridge, C. W. & Waterhouse, B. D. The locus coeruleus–noradrenergic system: modulation of behavioral state and state-dependent cognitive processes. *Brain Res. Brain Res. Rev.* **42**, 33–84 (2003).
35. Audet, M. A., Doucet, G., Oleskevich, S. & Descarries, L. Quantified regional and laminar distribution of the noradrenaline innervation in the anterior half of the adult rat cerebral cortex. *J. Comp. Neurol.* **274**, 307–318 (1988).
36. O'Donnell, J., Zeppenfeld, D., McConnell, E., Pena, S. & Nedergaard, M. Norepinephrine: a neuromodulator that boosts the function of multiple cell types to optimize CNS performance. *Neurochem. Res.* **37**, 2496–2512 (2012).
37. Kohm, A. P. & Sanders, V. M. Norepinephrine and beta 2-adrenergic receptor stimulation regulate CD4+ T and B lymphocyte function in vitro and in vivo. *Pharm. Rev.* **53**, 487–525 (2001).

38. Orr, A. G., Orr, A. L., Li, X. J., Gross, R. E. & Traynelis, S. F. Adenosine A_{2A} receptor mediates microglial process retraction. *Nat. Neurosci.* **12**, 872–878 (2009).
39. Bernier, L. P. et al. Nanoscale surveillance of the brain by microglia via cAMP-regulated filopodia. *Cell Rep.* **27**, 2895–2908.e2894 (2019).
40. Eyo, U. B. et al. Modulation of microglial process convergence toward neuronal dendrites by extracellular calcium. *J. Neurosci.* **35**, 2417–2422 (2015).
41. Zhao, X., Eyo, U. B., Murugan, M. & Wu, L. J. Microglial interactions with the neurovascular system in physiology and pathology. *Dev. Neurobiol.* **78**, 604–617 (2018).
42. Li, Y., Du, X. F., Liu, C. S., Wen, Z. L. & Du, J. L. Reciprocal regulation between resting microglial dynamics and neuronal activity in vivo. *Dev. Cell* **23**, 1189–1202 (2012).
43. Chan-Palay, V. & Asan, E. Alterations in catecholamine neurons of the locus coeruleus in senile dementia of the Alzheimer type and in Parkinson's disease with and without dementia and depression. *J. Comp. Neurol.* **287**, 373–392 (1989).
44. Kvetnansky, R., Sabban, E. L. & Palkovits, M. Catecholaminergic systems in stress: structural and molecular genetic approaches. *Physiol. Rev.* **89**, 535–606 (2009).
45. Heneka, M. T. et al. Locus ceruleus controls Alzheimer's disease pathology by modulating microglial functions through norepinephrine. *Proc. Natl Acad. Sci. USA* **107**, 6058–6063 (2010).
46. Xu, H., Rajsombath, M. M., Weikop, P. & Selkoe, D. J. Enriched environment enhances beta-adrenergic signaling to prevent microglia inflammation by amyloid-beta. *EMBO Mol. Med.* **10**, e8931 (2018).
47. Hong, S. et al. Complement and microglia mediate early synapse loss in Alzheimer mouse models. *Science* **352**, 712–716 (2016).
48. Mitchell, H. A. & Weinshenker, D. Good night and good luck: norepinephrine in sleep pharmacology. *Biochem. Pharm.* **79**, 801–809 (2010).
49. Brown, E. N., Lydic, R. & Schiff, N. D. General anesthesia, sleep, and coma. *N. Engl. J. Med.* **363**, 2638–2650 (2010).

Acknowledgements

This work is supported by the National Institutes of Health (R01NS088627, R21DE025689 and R01NS112144 to L.-J.W.) and by a postdoctoral fellowship from the Mayo Clinic Center for Multiple Sclerosis and Autoimmune Neurology (to T.C). The authors thank M. Mattson (National Institute on Aging) for critical reading of the paper and members of the Wu Lab at the Mayo Clinic for insightful discussions.

Author contributions

Y.U.L., H.D. and L.-J.W. designed the studies. Y.U.L., A.D.U. and L.-J.W. wrote and revised the manuscript. Y.U.L. performed the electrophysiology experiments. Y.U.L., Y.Y., Y.L., U.B.E., T.C., J. Zheng, A.D.U., J .Zhu and D.B.B. performed animal surgery, image collection and data analyses. Y.U.L. and J. Zheng performed the in situ hybridization and immunofluorescence staining experiments.

Competing interests

The authors declare no competing interests.

Additional information

Supplementary information is available for this paper at https://doi.org/10.1038/s41593-019-0511-3.

Correspondence and requests for materials should be addressed to L.-J.W.

Reprints and permissions information is available at www.nature.com/reprints.

Publisher's note Springer Nature remains neutral with regard to jurisdictional claims in published maps and institutional affiliations.

Methods

Animals. Male and female mice, 2–3 months of age, were used in accordance with institutional guidelines. All experiments were approved by the Mayo Clinic Animal Care and Use Committee. Heterozygous *Cx3cr1*$^{GFP/+}$ were used for all experiments[50]. *P2y12*$^{-/-}$ mice were originally donated by M. Dailey at the University of Iowa. The following mice were purchased from the Jackson Laboratory: heterozygous R26-LSL-Gi-DREADD (Gi-DREADD; 026219); transgenic *VGAT-ChR2* (014548); and R26-LSL-tdTomato reporter mice (td-Tomato; 007909). Heterozygous Gi-DREADD mice were bred to homozygous *Cx3cr1*$^{GFP/GFP}$ mice to obtain Gi-DREADD-positive and -negative (sibling control) offspring for experiments. Transgenic *VGAT-ChR2* mice were also bred to homozygous *Cx3cr1*$^{GFP/GFP}$ mice to obtain offspring with (TG) and without (non-TG control) transgene expression. Finally, *P2y12*$^{-/-}$ mice were bred to *P2y12*$^{-/-}$:*Cx3cr1*$^{GFP/GFP}$ mice to obtain *P2y12*$^{-/-}$:*Cx3cr1*$^{GFP/+}$ animals for imaging studies. *Thy1-YFP* mice (Jackson Laboratory, 003782) were bred to *Cx3cr1*$^{GFP/GFP}$ to obtain *Cx3cr1*$^{GFP/+}$:*Thy1-YFP* to observe physical interactions between microglial processes and neuronal dendrites. Animals used for all experiments were randomly selected.

Virus injection. To image neuronal network activity in vivo, 0.3 µl of AAV9.CamKII.GCaMP6s (G12289, Penn Vector Core) was injected into the somatosensory cortex (2-mm posterior and 1.5-mm lateral to bregma) or the barrel cortex (1.45-mm posterior and 3-mm lateral to bregma). To specifically target noradrenergic neurons, 0.3 µl of AAV9.rTH. Cre (G12845, Penn Vector Core) was injected into the LC (5.4-mm posterior, 0.9-mm lateral and 3.7-mm ventral to bregma) of Gi-DREADD or td-Tomato mice bred with *Cx3cr1-GFP*. To express Gq-DREADD in noradrenergic neurons, we injected the following cocktail of three viruses into the LC of *Cx3cr1*$^{GFP/+}$ mice: AA9.rTH.PI.Cre, AAV9.DIO.hM3D(Gq) (44361, Addgene) and AAV9.FLEX.tdTomato (28306, Addgene).

Chronic window implantation. Mice were implanted with a chronic cranial window as previously described[15]. Briefly, mice were anesthetized with isoflurane (3% induction, 1.2% maintenance) and maintained on a heating pad during surgery. A dental drill (Osada Model EXL-M40) was used to drill a circular >3-mm diameter craniotomy. For the limb/trunk region of the somatosensory cortex, the craniotomy center was approximately 2-mm posterior and 1.5-mm lateral to bregma. For the barrel cortex, the craniotomy center was approximately −1.45-mm posterior and ±3-mm lateral to bregma. A 3-mm glass coverslip previously sterilized in 70% ethanol was placed inside the craniotomy, then light-curing dental cement (Tetric EvoFlow) was applied around the glass coverslip and cured with a Kerr Demi Ultra LED Curing Light (Dental Health Products). The skull, excluding the region with the window, was then covered with IBond Total Etch glue (Heraeus) and cured with light-emitting diode light. Finally, a custom-made head bar was attached to the skull using light-curing dental glue. Mice were allowed to recover from anesthesia on a heating pad for 10 min before they were returned to their home cage. Ibuprofen in drinking water was provided as an analgesic for 48 h post-surgery.

In vivo two-photon imaging. After recovery from cranial window surgery (2–4 weeks), mice were trained to freely move on a custom-made, rotating treadmill while head restrained (Supplementary Fig. 1a,b) for 3 days (2 sessions per day, 10 min per session). On the day of imaging, all mice with a clear, chronic glass window were included (approximately 50% of mice with attenuated window quality were excluded before any data collection). Mice were imaged using a two-photon imaging system (Scientifica) equipped with a tunable Ti:Sapphire Mai Tai DeepSee laser (Spectra Physics). Laser wavelength was tuned to 900 nm to image *Cx3cr1*$^{GFP/+}$ microglia, 920 nm to image GCaMP6s fluorescence or 950 nm to image tdTomato-labeled LC projections. Imaging utilized a ×40 water-immersion lens and a 180 × 180 µm field of view (512 × 512 pixel resolution). The microscope was equipped with a 565-nm dichroic mirror and the following emission filters: 525/50 nm (green channel) and 620/60 nm (red channel) for GFP/tdTomato imaging and a 509-nm dichroic mirror with 500/15 nm (green channel) and 537/26- nm (red channel) emission filters for GFP and yellow fluorescent protein (YFP) imaging. The laser power was maintained at 30–40 mW. Imaging in the cortex was conducted 50–150 µm beneath the pial surface. To induce general anesthesia in awake mice, isoflurane (3% for initiation, 1.2% for maintenance) was introduced through an anesthesia nose cone. Ketamine/xylazine (87.5 mg per kg ketamine, 12.5 mg per kg xylazine) and urethane (1.6 mg per kg) were administered through intraperitoneal injection. The body temperature of anesthetized mice was maintained at 37 °C by a heating pad. To image microglial dynamics, we acquired *z*-stack images (8 sections, 2-µm step size) once every minute (Supplementary Fig. 1c). When selecting the *z*-stack area, we focused on areas of the cortex in which approximately three microglial somas resided at a consistent *z*-level and had processes that could be incorporated in the *x*–*y* imaging plane. The *z*-stack range was then set so that microglial somas represented the approximate center of the *z*-range. All microglia preselected by these unbiased criteria were then analyzed. For calcium imaging, continuous acquisition (1-Hz time series) was carried out approximately 60 µm from the pial surface to study neuronal process calcium activity in layer 1, or approximately 150 µm from the pial surface to study neuronal soma calcium activity in layer 2/3. For laser injury, we focused the laser at ×66magnification and held it at ~250 mW for 1 s at an 800-nm wavelength. For imaging microglia–neuron interactions, we used a GFP/YFP filter set and the same acquisition protocol as microglial surveillance studies. Data collection was not performed blinded to the conditions of the experiments.

Drug application in vivo. Intracerebral administration of neurotransmitters or antagonists was carried out through a catheter implanted 2 weeks after the chronic window implantation surgery (Fig. 3a, left panel). The catheter was carefully placed in the subarachnoid space through the cisterna magna and close to the imaging window. We verified that dye can defuse through the catheter to the imaging window within seconds of infusion. The catheter was filled with ACSF to maintain patency, and no microglia activation was observed within the area of the window after implantation. A total volume of 10 µl of solution was applied through the catheter and into the brain. Neurotransmitters were exogenously applied at the following concentrations: 5 mM acetylcholine chloride, 1 mM dopamine hydrochloride, 3 mM NE and 5 mM serotonin hydrochloride. The dose of muscimol (870 µM) and TTX (10 µM) represents the minimal dose needed to induce significant suppression of neuronal activity. CNO was intraperitoneally injected at 5 mg per kg to activate Gi-DREADD in awake mice.

Imaging data analyses. Images were analyzed using ImageJ[51]. All microglia preselected via unbiased inclusion criteria were then analyzed. Inclusion criteria included a clearly identifiable soma near the center of the *z*-stack and multiple processes incorporated within the *x*–*y* imaging plane. Because rapid movements by the animal could lead to image distortion in the *x*–*y* plane, five images were sequentially acquired at each *z*-level (Supplementary Fig. 1c). At each *z*-level, the user selected the image with the least distortion for inclusion in a 'sorted' *z*-stack (Supplementary Fig. 1d). Images in this *z*-stack were then aligned along the *z* axis using the StackReg plugin to create a final *z*-stack used in analyses.

To obtain the total process area value, a maximum-intensity projection (MIP) along the *z* axis was then created from the final *z*-stack. After applying a uniform threshold to the MIP images, the Analyze particles tool was used to derive a process area value from this flattened image. To obtain a process surveillance territory value, a bounding box connecting the distal-most edges of the microglial processes was then mapped onto the MIP image. The area encompassed within this bounding box was defined as the microglial surveillance territory. Area and territory values in subsequent stacks were normalized to the values of the first stack to determine changes over time. Process velocity was measured using the Manual tracking plugin. Sholl analysis was performed in ImageJ with the Sholl analysis plugin. *Z*-stacks acquired between the 10 and 20 min mark were used to evaluate microglial dynamics in the awake condition. *Z*-stacks acquired between the 20 and 30 min mark after anesthesia (isoflurane, ketamine/xylazine and urethane) were used to evaluate microglial dynamics in the anesthetized conditions. Similarly, *z*-stacks acquired between the 20 and 30 min mark were also used for analyses following all other manipulations: pharmacological, chemogenetic, optogenetic or sensory deprivation. For evaluating neuronal activity, calcium values above a set threshold ($\Delta F/F > 0.2$) were summated in 1-min bins and reported as the normalized change in sum relative to the first minute (Fig. 1; Supplementary Fig. 3). Alternatively, the same value was summated across a 10-min period before and after either whisker trimming (Supplementary Fig. 5a–c) or muscimol administration (Supplementary Fig. 6).

To analyze interactions between microglial processes and neuronal dendrites, we calculated physical contact duration and the area of contact once per minute throughout a 30-min recording in the awake animal. Under anesthesia conditions, we performed identical measurements between 30 and 60 min after anesthesia. Contact area between microglial processes and dendrites was normalized to the mean area of overlap determined during the first 10 min of recording in the awake condition. Data analysis was performed blinded to the conditions of the experiments.

Electrophysiology. For verification of ChR2 function in VGAT-positive neurons or of Gi-DREADD function in noradrenergic neurons, we studied single-cell activity in transverse, acute brain slices (350 µm) containing either the somatosensory cortex (*VGAT-ChR2* mice) or the LC (Gi/Gq-DREADD-expressing mice). Transverse or sagittal brain slices were cut in chilled (2–4 °C) cutting solution containing the following (in mM): 185 sucrose, 2.5 KCl, 1.2 NaH_2PO_4, 25 $NaHCO_3$, 25 glucose, 10 $MgCl_2$ and 0.5 $CaCl_2$. Slices were then transferred to an incubator with ACSF containing the following (in mM): 130 NaCl, 2.5 KCl, 1.3 NaH_2PO_4, 26 $NaHCO_3$, 10 glucose, 2 $MgCl_2$, 2 $CaCl_2$ (pH 7.3–7.4; osmolarity: 300–310 mOsm; saturated with 95% O_2/5% CO_2 to provide stable pH and continuous oxygenation). For recovery, slices were kept at 29–30 °C for a 30-min period, then cooled and kept at room temperature for at least 1 h before recording. During recording, slices were continuously perfused with room temperature ACSF using a peristaltic bath perfusion system. Whole-cell recordings were performed using glass pipettes (3–5 MΩ) filled with the following intracellular solution containing (in mM): 121 KCl, 19 potassium-gluconate, 5 NaCl, 4 $MgCl_2$, 10 HEPES buffer, 0.1 EGTA, 4 Mg-ATP, Na_2-GTP (pH 7.3–7.4; osmolarity: 280–290 mOsm). Data were collected using a MultiClamp 700B amplifier (Molecular Devices). Signals were filtered at 2 kHz and digitized at 10 kHz with a Digidata 1550 Data Acquisition System and

analyzed using the software pCLAMP 10 (Molecular Devices) or Mini Analysis 6.0.3 (Synaptosoft).

For field potential recording in the somatosensory cortex in awake mice, a specialized recording headplate was adhered to the mouse 2 weeks before recording. Following 3 days of training on the treadmill platform, a craniotomy was made above the somatosensory cortex under general anesthesia, as described above, except that a smaller glass coverslip (2 mm in diameter) was affixed over part of the craniotomy to provide an unobstructed region for micropipette insertion and recording (Supplementary Fig. 2e). After recovery from the surgery, mice were head-fixed and allowed to move on the treadmill. A glass pipettes filled with ACSF containing Alexa-594 was inserted through the dura and into the cortex under two-photon guidance. Data were acquired continuously in the awake and anesthetized conditions using the parameters described above for single-cell recording.

Two-photon imaging of acute brain slices. Transverse brain slices were used for microglial imaging. Acute brain slices were prepared as described above in the "Electrophysiology" section. The imaging protocol was the same as described above for "In vivo two-photon imaging", except with modified imaging stack parameters (100–140 µm in depth, 2-µm step size). Data analyses from slice imaging are the same as for the in vivo experiments. Drugs were applied in a bath. To prepare isoflurane-enriched ACSF, carbogen gas was passed through an Anesthetic Vaporizer (Midmark Matrix, VIP 3000) at a constant flow rate of 500 ml min^{-1} and then bubbled through the ACSF reservoir.

RNAscope in situ hybridization and immunohistofluorescence staining. To visualize β_2-adrenergic receptor (*Adrb2*) mRNA in situ, a RNAscope 2.5 HD Detection kit (Advanced Cell Diagnostics, 322360) was applied in accordance with the manufacturer's protocol using fixed, frozen sections of 10-µm thickness. Briefly, sections were first dried for 30 min at 60 °C and cleared of OCT embedding matrix via a 5-min PBS wash. During pretreatment, the sections were incubated in hydrogen peroxide for 10 min at room temperature. Then the slides were submerged in 1× target retrieval solution for 5 min at 98–102 °C. After antigen retrieval, the slides were immediately transferred to distilled water and rinsed three to five times. Wash steps were then repeated with 100% ethanol. The sections were incubated in Protease Plus for protein digestion at 40 °C for 30 min. To run the assay, the RNAscope Probe Mm-Adrb2 (449771) was applied on pretreated sections for 120 min at 40 °C. After probe hybridization, the signal was amplified by incubation with amplifier 1–6 in sequence. Each incubation step was followed by two 2-min washes using washing buffer. To visualize the hybridized signal, 2.5 HD Detection Reagent-RED (322360) was applied onto the sections for 10 min at room temperature. The sections were rinsed in fresh tap water before observation. To further determine *Adrb2* expression in microglia, the assay was continued with a modified immunofluorescence staining protocol following the manufacturer's instructions. Fluorescent images were acquired using a confocal microscope (Zeiss LSM-810). Cells that were positive for IBA1 (Wako, 019-19741, 1:500 dilution) and colocalized with two or more mRNA puncta were counted as positive.

Statistical analyses. Statistical analyses utilized a paired *t*-test design with a two-tailed test of significance for changes within a cell across conditions. Comparisons between genotypes utilized an unpaired *t*-test design with a two-tailed test of significance. D'Agostino–Pearson tests were used to assess normality before applying a parametric or nonparametric *t*-test variant (paired: Wilcoxon matched-pairs rank test; unpaired: Mann–Whitney test). One-way analysis of variance (ANOVA) was used to compare three groups. All statistical testing was performed using GraphPad Prism (GraphPad Software). Data distribution was assumed to be normal, but this was not formally tested. Data are shown as individual values or expressed as the mean ± s.e.m. when grouped. A P value < 0.05 was considered statistically significant. All P values that are not less than 0.0001 are provided as exact values, otherwise they are indicated as $P < 0.0001$. No statistical methods were used to predetermine sample sizes, but our sample sizes were similar to those reported in previous publications[13,14].

Please see the Nature Research Reporting Summary for information about the reproducibility of our work.

Reporting Summary. Further information on research design is available in the Nature Research Reporting Summary linked to this article.

Data availability

Source data for all graphs are available from the corresponding author upon request.

References

50. Jung, S. et al. Analysis of fractalkine receptor CX(3)CR1 function by targeted deletion and green fluorescent protein reporter gene insertion. *Mol. Cell. Biol.* **20**, 4106–4114 (2000).
51. Schindelin, J. et al. Fiji: an open-source platform for biological-image analysis. *Nat. Methods* **9**, 676–682 (2012).

nature research

Corresponding author(s): Long-Jun Wu

Last updated by author(s): Sep 1, 2019

Reporting Summary

Nature Research wishes to improve the reproducibility of the work that we publish. This form provides structure for consistency and transparency in reporting. For further information on Nature Research policies, see Authors & Referees and the Editorial Policy Checklist.

Statistics

For all statistical analyses, confirm that the following items are present in the figure legend, table legend, main text, or Methods section.

n/a	Confirmed	
☐	☒	The exact sample size (*n*) for each experimental group/condition, given as a discrete number and unit of measurement
☐	☒	A statement on whether measurements were taken from distinct samples or whether the same sample was measured repeatedly
☐	☒	The statistical test(s) used AND whether they are one- or two-sided *Only common tests should be described solely by name; describe more complex techniques in the Methods section.*
☐	☒	A description of all covariates tested
☐	☒	A description of any assumptions or corrections, such as tests of normality and adjustment for multiple comparisons
☐	☒	A full description of the statistical parameters including central tendency (e.g. means) or other basic estimates (e.g. regression coefficient) AND variation (e.g. standard deviation) or associated estimates of uncertainty (e.g. confidence intervals)
☐	☒	For null hypothesis testing, the test statistic (e.g. *F*, *t*, *r*) with confidence intervals, effect sizes, degrees of freedom and *P* value noted *Give P values as exact values whenever suitable.*
☒	☐	For Bayesian analysis, information on the choice of priors and Markov chain Monte Carlo settings
☒	☐	For hierarchical and complex designs, identification of the appropriate level for tests and full reporting of outcomes
☒	☐	Estimates of effect sizes (e.g. Cohen's *d*, Pearson's *r*), indicating how they were calculated

Our web collection on statistics for biologists contains articles on many of the points above.

Software and code

Policy information about availability of computer code

Data collection	ScanImage (Matlab based) for two-photon imaging acquisition; Axon 700B and pClamp10 for electrophysiological data collection.
Data analysis	ImageJ v1.52i (Fiji) for two-photon images analysis; Software Clampfit 10, Mini Analysis 6.0.3 for electrophysiological data analysis; GraphPad Prism 7 for figures and statistics.

For manuscripts utilizing custom algorithms or software that are central to the research but not yet described in published literature, software must be made available to editors/reviewers. We strongly encourage code deposition in a community repository (e.g. GitHub). See the Nature Research guidelines for submitting code & software for further information.

Data

Policy information about availability of data

All manuscripts must include a data availability statement. This statement should provide the following information, where applicable:

- Accession codes, unique identifiers, or web links for publicly available datasets
- A list of figures that have associated raw data
- A description of any restrictions on data availability

Source data for all graphs are available from the corresponding authors upon request.

Field-specific reporting

Please select the one below that is the best fit for your research. If you are not sure, read the appropriate sections before making your selection.

☒ Life sciences ☐ Behavioural & social sciences ☐ Ecological, evolutionary & environmental sciences

Life sciences study design

All studies must disclose on these points even when the disclosure is negative.

Sample size	No statistical methods were used to pre-determine sample sizes but our sample sizes are similar to those reported in previous publications (Nimmerjahn et al., Science 2005; Davalos et al., Nat Neurosci 2005)
Data exclusions	No data were excluded from the analyses.
Replication	All the mice with success chronic cranial glass windows surgery were used for imaging and replicated all the results described in the manuscript. The results were replicated by at least two investigators in our lab.
Randomization	All cells analyzed were randomly selected from in vivo and in vitro samples.
Blinding	The investigator for imaging collection was not blind to mice group, but the investigator for imaging analysis was blind to mice group and treatments.

Reporting for specific materials, systems and methods

We require information from authors about some types of materials, experimental systems and methods used in many studies. Here, indicate whether each material, system or method listed is relevant to your study. If you are not sure if a list item applies to your research, read the appropriate section before selecting a response.

Materials & experimental systems

n/a	Involved in the study
☒	☐ Antibodies
☒	☐ Eukaryotic cell lines
☒	☐ Palaeontology
☐	☒ Animals and other organisms
☒	☐ Human research participants
☒	☐ Clinical data

Methods

n/a	Involved in the study
☒	☐ ChIP-seq
☒	☐ Flow cytometry
☒	☐ MRI-based neuroimaging

Animals and other organisms

Policy information about studies involving animals; ARRIVE guidelines recommended for reporting animal research

Laboratory animals	C57BL/6, male and female, 2-4 months old; transgenic mice: CX3CR1-GFP/+, CX3CR1-GFP/GFP, P2Y12-/-: CX3CR1-GFP/+; Gi-DREADD-flox/+:CX3CR1-GFP/+, tdTomato-flox/+:CX3CR1-GFP/+, Thy1-YFP: CX3CR1-GFP/+
Wild animals	No wild animals were used in this study.
Field-collected samples	No field-collected samples were used in this study.
Ethics oversight	We performed all procedures involving live mice in accordance with the NIH Guide for the Care and Use of Laboratory Animals and the protocols approved by the . All experiments were approved by the Mayo Clinic Animal Care and Use Committee.

Note that full information on the approval of the study protocol must also be provided in the manuscript.